

Article

Synthesis and Electrochemical Properties of TiNb_2O_7 and $\text{Ti}_2\text{Nb}_{10}\text{O}_{29}$ Anodes under Various Annealing Atmospheres

Touraj Adhami ¹, Reza Ebrahimi-Kahrizsangi ^{1,*}, Hamid Reza Bakhsheshi-Rad ^{1,*}, Somayeh Majidi ², Milad Ghorbanzadeh ³ and Filippo Berto ⁴

¹ Advanced Materials Research Center, Department of Materials Engineering, Najafabad Branch, Islamic Azad University, 1477893855 Najafabad, Iran; t.adhami20@gmail.com

² Department of Chemistry, Najafabad Branch, Islamic Azad University, 1477893855 Najafabad, Iran; somaye.majidi2010@gmail.com

³ Materials and Energy Research Center, 14155-4777 Karaj, Iran; milad.ghorbanzadeh@gmail.com

⁴ Department of Mechanical and Industrial Engineering, Norwegian University of Science and Technology, 7491 Trondheim, Norway; filippo.berto@ntnu.no

* Correspondence: rezaebrahimi@iaun.ac.ir (R.E.-K.); rezabakhsheshi@gmail.com (H.R.B.-R.)

Abstract: In this study, two compounds of TiNb_2O_7 and $\text{Ti}_2\text{Nb}_{10}\text{O}_{29}$ were successfully synthesized by mechanochemical method and post-annealing as an anode material for lithium-ion batteries. The effect of annealing atmosphere on the morphology, particle size, and electrochemical characteristics of two compounds was investigated. For these purposes, the reactive materials were milled under an argon atmosphere with a certain mole ratio. Subsequently, each sample was subjected to annealing treatment in two different atmospheres, namely argon and oxygen. Phase and morphology identifications were carried out by X-ray diffraction (XRD) and field emission scanning electron microscopy (FESEM) to identify the phases and evaluate the morphology of the synthesized samples. The charging and discharging tests were conducted using a battery-analyzing device to evaluate the electrochemical properties of the fabricated anodes. Annealing in different atmospheres resulted in variable discharge capacities so that the two compounds of TiNb_2O_7 and $\text{Ti}_2\text{Nb}_{10}\text{O}_{29}$ annealed under the argon atmosphere showed a capacity of 60 and 66 mAh/g after 179 cycles, respectively, which had a lower capacity than their counterpart under the oxygen atmosphere. The final capacity of the annealed samples in the oxygen atmosphere is 72 and 74 mAh/g, respectively.

Keywords: lithium-ion batteries; electrode materials; annealing; electrochemical; mechanochemical processing



Citation: Adhami, T.; Ebrahimi-Kahrizsangi, R.; Bakhsheshi-Rad, H.R.; Majidi, S.; Ghorbanzadeh, M.; Berto, F. Synthesis and Electrochemical Properties of TiNb_2O_7 and $\text{Ti}_2\text{Nb}_{10}\text{O}_{29}$ Anodes under Various Annealing Atmospheres. *Metals* **2021**, *11*, 983. <https://doi.org/10.3390/met11060983>

Received: 28 April 2021

Accepted: 16 June 2021

Published: 20 June 2021

Publisher's Note: MDPI stays neutral with regard to jurisdictional claims in published maps and institutional affiliations.



Copyright: © 2021 by the authors. Licensee MDPI, Basel, Switzerland. This article is an open access article distributed under the terms and conditions of the Creative Commons Attribution (CC BY) license (<https://creativecommons.org/licenses/by/4.0/>).

1. Introduction

Recently, global warming and energy saving are among the most crucial issues in the world. Moreover, with rapid economic growth and manpower, global energy consumption increases dramatically [1–3]. Thus, the issue of sustainability and saving energy resources worldwide received great consideration due to the crisis of reducing and terminating fossil energy resources and consideration of environmental pollution issues [4]. Among energy-saving systems, batteries are one of the types of energy storage systems that currently have a wide range of commercial or underdeveloped research stages [5]. Lithium-ion (Li-ion) batteries with increased effectiveness, lower costs, and increased safety are required for a variety of applications, such as hybrid cars, consumer electronics, and grid-scale energy storage, and considerable research and development initiatives are underway [6–8]. In the field of lithium-ion battery electrode materials research, efforts were made to replace the traditional Li-graphite (LiC_6) anode with novel compounds that address its drawbacks. In actuality, an SEI (solid–electrolyte interface) film is needed to passivate that anode in order to avoid redox interactions with the liquid–carbonate electrolyte, with the unintended consequence of probable lithium dendrite formation, which might short-circuit the cell and

ignite the electrolyte. Hence, anodes having a greater voltage vs. Li^+/Li than LiC_6 (0.2V), frequently around 1V, are preferred to prevent the risk of interacting with the electrolyte without the requirement for the inconvenient SEI film [9–12]. Anodes are among the most vital elements in producing batteries so that they determine the electrochemical nature and the capacity of batteries [5]. Hence, regarding the rapid growth of the world population and more extensive need to the energy resources and saving it, research and development of anode materials employed in the batteries with lithium-ion with high capacity and proper cyclability and the intermediate metal oxides are seriously studied [13,14]. These two compounds, i.e., TiNb_2O_7 and $\text{Ti}_2\text{Nb}_{10}\text{O}_{29}$, were considered by many researchers [15–20] due to their unique characteristics such as high theoretical capacities of 387 and 400 mAh/g (much more than $\text{Li}_4\text{Ti}_5\text{O}_{12}$: 175 mAh/g), the process of rapid insertion and extraction of lithium ion owing to rapid reaction kinetics, and high operating voltage (~1.6 sv, Li/Li^+) which can prevent the formation of the solid electrolyte interface (SEI) layer. However, the operating discharge of these materials is not quite satisfactory due to their weak electric conductivity and the slow rate of ion transfer [15,16,21]. Various approaches and strategies, including reducing the particles size and improving the specific area, and designing the porous structures, were investigated to address this issue, since a higher ratio of area to the volume shortens the distance for penetration of lithium ions, improves the electric conductivity, and will consequently improve the lithium ions storage performance [13,16]. For instance, X. Xia et al. [16] successfully fabricated an electrode of $\text{Ti}_2\text{Nb}_{10}\text{O}_{29}$ nano-porous spheres via the method, and their result exhibited that the capacity of 215 mAh/g after 500 cycles with C rate = 10 C. In this context, it is worth noting that the fabrication method and subsequent controlling annealing atmosphere significantly affect the crystal size of particles and lithium ions penetration. Several variables in this process can influence the structure and morphology of the particles. One of the existing most influential parameters in the annealing treatment is the type of annealing atmosphere. Nowadays, the synthesis methodology, together with the process of materials properties transfer in different atmospheres, is a fixed method [22,23]. Hansen et al. investigated the dynamic reversible deformation in different nanocrystals in various atmospheres [24]. Research shows that the capacity of TiO_2 electrodes is greatly dependent on the annealing parameters such as temperature [25,26], pressure [27], and atmosphere [28,29]. However, there is no report, regarding the importance of the effect of annealing atmosphere, on the electrochemical properties of TiNb_2O_7 and $\text{Ti}_2\text{Nb}_{10}\text{O}_{29}$ anodes. Thus, this study evaluated the synthesis and analysis of the two compositions of TiNb_2O_7 and $\text{Ti}_2\text{Nb}_{10}\text{O}_{29}$ by the mechanical alloying together with the annealing treatment under the two different atmospheres, namely argon and oxygen. Furthermore, the influence of annealing atmosphere on the particle size, morphological changes, and electrochemical performance, including the capacity and cyclability of the fabricated anode-based TiO_2 and Nb_2O_5 , are evaluated.

2. Materials and Methods

2.1. TiNb_2O_7 and $\text{Ti}_2\text{Nb}_{10}\text{O}_{29}$ Synthesis

Commercial oxides TiO_2 ($\geq 99\%$, Merck, Darmstadt, Germany) and Nb_2O_5 (99.5%, Merck, Darmstadt, Germany) with a particle size of about 25 μm were prepared to produce ceramic powders. To perform the process, materials with a specific molar ratio based on the reactions 1 and 2 according to Ref. [9] were milled in a planetary ball mill consisting of a chamber and steel balls for 5 h under an argon atmosphere at a rotational speed of 600 rpm. In all experiments, the ball to powder ratio (BPR) was 15 to 1.



Subsequently, in order to complete the reaction, a tube furnace was used for annealing the milled materials under two different atmospheres of oxygen and argon. In this opera-

tion, the materials were annealed at 900 °C for 2 h. Table 1 shows the specifications of the applied parameters in the test process.

Table 1. Specifications of the applied parameters in the experimental process.

Sample No.	Stoichiometric Reaction	Milling Time (h)	Furnace/Annealing Atmosphere	Annealing Time (h)	Annealing Temperature (°C)
S1	TiNb ₂ O ₇	5	Tube/oxygen	2	900
S2	TiNb ₂ O ₇	5	Tube/argon	2	900
S3	Ti ₂ Nb ₁₀ O ₂₉	5	Tube/oxygen	2	900
S4	Ti ₂ Nb ₁₀ O ₂₉	5	Tube/argon	2	900

2.2. Material Characterization

The study of the formed phases was performed by X-ray diffraction (XRD, Philips PW3040, Netherlands). The beam Cu K α ($\lambda = 1.54056 \text{ \AA}$) was used to perform the analysis. The bounce rate was chosen to be 1 degree per minute, the operating voltage was 30 kV, the current was 30 mA, and the scattering angle (2θ) was 15 to 80. Field emission electron microscopy (FE-SEM, Tescan MIRA3, Czech Republic) was used to study the morphology and size of the product particles. Then, to evaluate the electrochemical performance, the slurry was evenly coated on a copper foil and placed in a vacuum oven at 120 °C for 12 h. Additionally, the Williamson–Hall equation was used to calculate the size of crystalline grains and their relationship to the annealing atmosphere, as presented in Equation (3) [30]:

$$b^2 \cos^2 \theta = \left(\frac{0.91\lambda}{D} \right)^2 + 4e^2 \sin^2 \theta \quad (3)$$

In this regard, b^2 is the peak width in radians. λ , D , and e , are the X-ray wavelength (Cu-K α $\lambda = 1.54056 \text{ \AA}$), crystal grain size, the lattice strain, and half the scattering angle of X-ray, respectively.

2.3. Electrochemical Characteristics

Lithium-ion storage performance in the compositions of TiNb₂O₇ and Ti₂Nb₁₀O₂₉ was investigated using the Li/TiNb₂O₇ and Li/Ti₂Nb₁₀O₂₉ half-cells. The working electrodes were produced by mixing each of the synthesized materials with polyvinylidene fluoride (PVDF) and black carbon as the adhesive and conductor with a weight ratio of 70:15:15 inside N-merhyl-2-pyrrolidone (MNP). The resulted slurry covered a copper foil and then dried inside an oven under vacuum condition for 12 h in the temperature of 120 °C. The anode material was loaded in each half-cell at a rate of 1 mg/cm² according to the Ref. [31]. A polypropylene film (Celgard 2400) was used in this study as a separator. Then, each of the prepared anodes were mounted within a standard vacuum glovebox with a pure lithium foil as a cathode or counter in the coin batteries (2032). The used electrolyte was prepared by the combination of one molar LiPF₆ in ethylene carbonate (EC), diethyl carbonate (DEC), and dimethyl carbonate (DMC) (with a volume ratio of 1:1:1). Charging and discharging tests were performed using a battery analyzer device by galvanostatic cycles in the voltage range of 0 to 3 volts at room temperature. In addition, in order to calculate the diffusion coefficient of lithium-ion in each cell and its relationship with the annealing atmosphere, an electrochemical impedance test was performed on each cell. The equation used to calculate the diffusion rate of lithium-ion is as follows [31]:

$$D = R^2 T^2 / 2A^2 n^4 F^4 C^2 \sigma_w^2 \quad (4)$$

where R is the gas constant (8.314 J/mol K), T is the absolute temperature, n is the number of electrons exchanged in each molecule during the redox process, A is the surface area of the electrode (1.77 cm²), C is the lithium-ion concentration ($7.69 \times 10^{-13} \text{ mol}\cdot\text{cm}^{-3}$), F

is the Faraday constant (96486 C/mol), ω is the angular frequency and σ_w is a Warburg factor that is directly related to Z' , as follows [31]:

$$Z' = R_e + R_{ct} + \sigma_w \omega^{-1/2} \quad (5)$$

where Z' is the real part of the electrochemical impedance test, indicating the general resistance of the cell, R_e represents the resistances due to the electrode and electrolyte, and R_{ct} is the charge transfer resistance.

3. Results and Discussion

3.1. Structure and Morphology

The morphology of the annealed samples under different atmospheres is shown in Figure 1. The investigations morphologically show that there is no difference between the annealed TNA compounds under oxygen and argon atmospheres. Therefore, the annealing atmosphere might be an effect on the morphology and crystallite size. It is worth noting that the particle size is in the range of 49 to 65 nm. On the other hand, the crystallite size obtained from the XRD patterns is approximately 49 nm based on the Williamson–Hall method. Thus, considering the proximity of these numbers to each other, it can be concluded that these values are the same as crystallite size. The EDS analysis of all specimens is further confirmed that the presence of Ti, Nb, and O representing the formation of $TiNb_2O_7$ and $Ti_2Nb_{10}O_{29}$ compounds as shown in Figure S1 (Supplementary Materials: Supporting Information).

Analysis of the obtained differential patterns shows that after the annealing treatment under both argon and oxygen atmosphere, the sample product formed as a result of the first reaction included the phases: $TiNb_2O_7$ (JCPDS 01-070-2009) and $Ti_2Nb_{10}O_{29}$ (JCPDS 01-072-0158) and the result of the second reaction was only single-phase ($Ti_2Nb_{10}O_{29}$) as shown in Figure 2. Annealing in the argon atmosphere produces oxygen-deficient compounds. Therefore, according to the stoichiometry of reaction 1 and the Rietveld refinements, the two XRD peaks at $2\theta \approx 25\text{--}27^\circ$ are the fingerprints of the $Ti_2Nb_{10}O_{29}$ phase. Although the product of all the annealed samples under different atmospheres was the same composition as $TiNb_2O_7$ and $Ti_2Nb_{10}O_{29}$, the displacement of the peaks could be seen in different samples. For instance, it can be seen that the annealed sample under oxygen has shifted towards a larger angle compared to that of under argon atmosphere. In general, the displacement of the peaks indicates a change in the degree of material disorder. In fact, the peak shifts may be due to changes in crystal lattice parameters or crystal size, which can be caused by annealing in different atmospheres. As a result, the structural defects (such as the changes in the crystal size and grain boundaries, vacant oxygen spaces, and the ratio of Ti^{+4}/Ti^{+3}) that occur in different annealing atmospheres can vary [32]. The impact of the annealing atmosphere on lithium storage performance in TNA compounds can be related to the changes in the crystal size. The size of the crystal grains may vary during the annealing process under different atmospheres, and the charge transfer and crystal stability properties may change accordingly. Thus, the difference in the crystal size of the material may make a difference in lithium storage performance [33]. FT-IR spectroscopy was examined to exhibit the bonding characteristics of the $TiNb_2O_7$ compound as shown in Figure S2 (Supplementary Materials: Supporting Information). As shown in the figure, the peaks at 924 and 530 cm^{-1} are attributed to the Nb-O-Nb stretching vibrations and the Nb-O-Nb bridging bonds, respectively. Ultimately, peaks at 694 and 839 cm^{-1} could be related to the stretching vibration of Ti-O-Ti bonds [34].

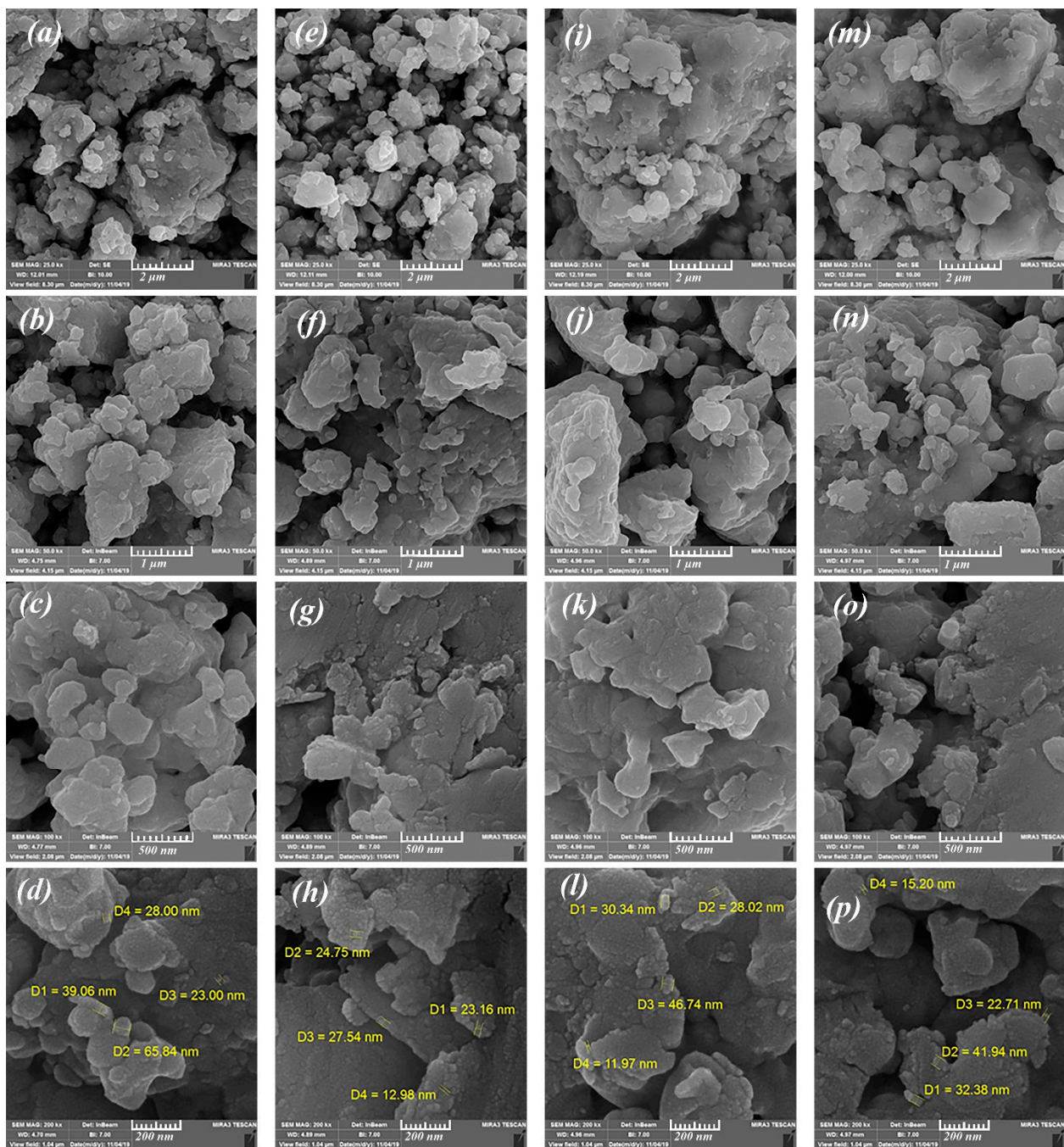


Figure 1. Images of FESEM microscope from the samples: (a–d) S1, (e–h) S2, (i–l) S3, and (m–p) S4 synthesized by ball milling under annealing treatment.

According to these studies, lithium insertion should be reduced by increasing the crystal size and vice versa. In other words, the amount of lithium input increases as the size of the crystal grains decreases, resulting in a shorter penetration path of the lithium-ion. The effect of an annealing atmosphere on lithium storage performance in TNA compounds can be related to the changes in the crystal structure. The parameters of a single cell and the size of a crystal may vary during the annealing process in different atmospheres, which may alter the properties of the transfer and structural stability. However, according to Figure 3, the particle size in the annealed samples in the oxygen atmosphere is greater compared to that in the argon atmosphere. In fact, larger samples have shown a greater ability to maintain capacity, which is inconsistent with the results reported by other researchers.

The reason for this can be attributed to lower compression and higher irregularity in the annealed samples under oxygen than argon [34–36]. Therefore, a more flexible structure is created that can accommodate more Li^+ and facilitate diffusion within this structure, which increases the retention of capacity in larger grain samples (in oxygen atmosphere). Structurally, the two phases of crystallography of TiNb_2O_7 and $\text{Ti}_2\text{Nb}_{10}\text{O}_{29}$ are part of a group of compounds known as Wadsley–Roth phases, in which, similar to the ReO_3 structure, they are interconnected by blocks that connect the octahedral space of oxygen and metal. TiNb_2O_7 consists of three broad octahedral spaces, and the regeneration of Ti^{+4} to Ti^{+3} and Nb^{+5} to Nb^{+4} with additional capacity is through the multi-electron reaction or excessive lithium generation. Insertion and extraction of lithium ions in the electrodes of TiNb_2O_7 and $\text{Ti}_2\text{Nb}_{10}\text{O}_{29}$ is performed by contacting the electrode with the electrolyte containing ions of Li^+ , as presented in Equations (6) [9] and (7) [21].

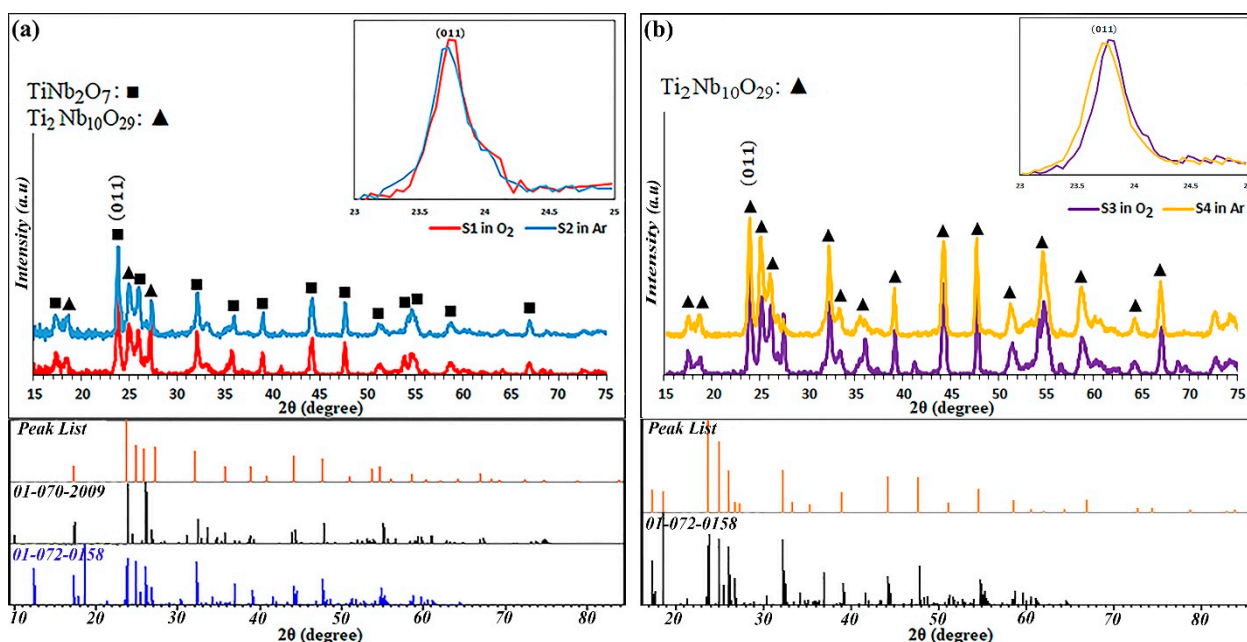


Figure 2. Diffracted X-ray patterns of the TiNb_2O_7 and $\text{Ti}_2\text{Nb}_{10}\text{O}_{29}$ compounds, annealed under different atmospheres (a) Peak shift of the (011) plane composition TiNb_2O_7 and (b) Peak shift of the (011) plane composition $\text{Ti}_2\text{Nb}_{10}\text{O}_{29}$.

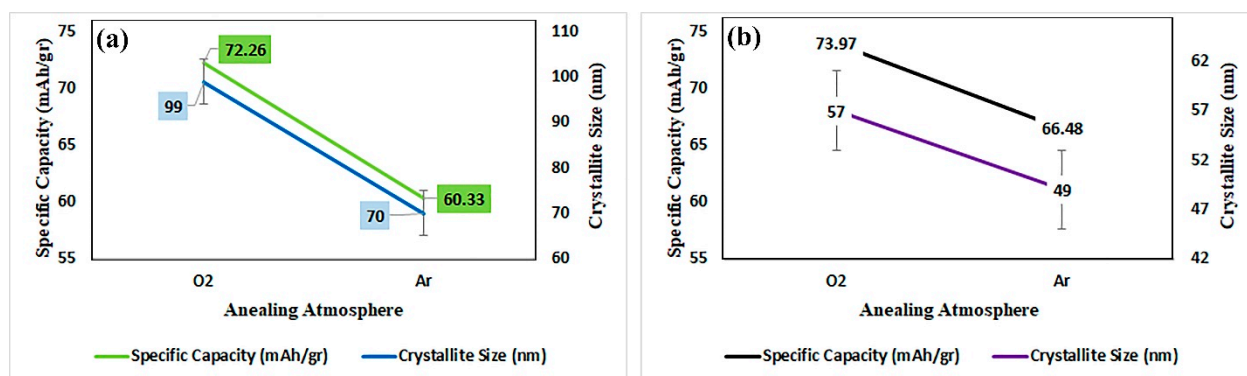


Figure 3. Comparison of the effect of annealing atmosphere on the crystal grain sizes and the specific capacity obtained X-ray diffraction data using the Williamson–Hall equation (a) TiNb_2O_7 , (b) $\text{Ti}_2\text{Nb}_{10}\text{O}_{29}$.

The annealed compounds under different atmospheres show a plateau area at 1.75 volts at charging and 1.6 volts at discharge time, although the values can change by the annealing atmosphere (Figure 4). The two plateau areas in the charging and discharging process can be due to the insertion and extraction of lithium ions in the interlayer and octahedral locations of TNA compounds.

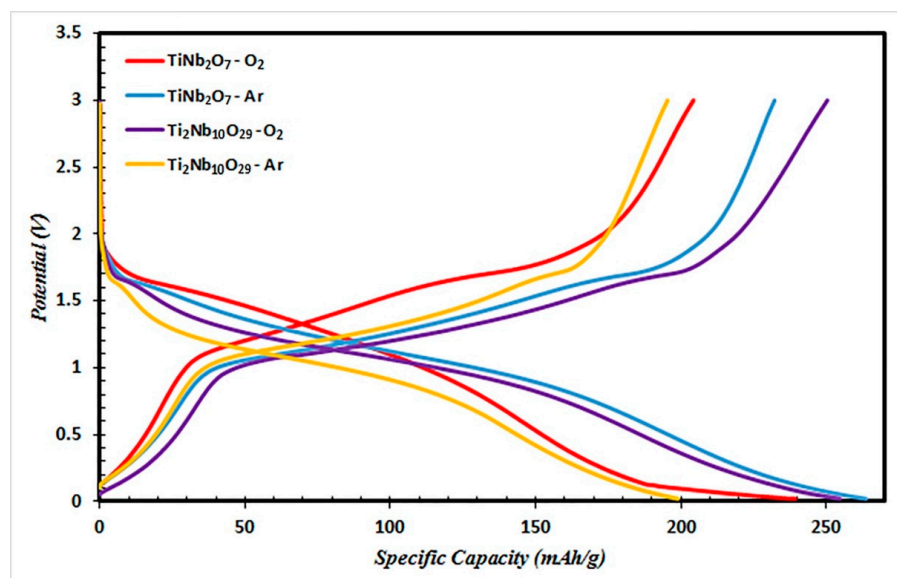


Figure 4. Charge/discharge curves of two synthesized samples in different atmospheres at 0.1 C cycled between 0 and 3 V.

Figure 5 shows the cyclability of both compounds in different atmospheres. Performing the annealing process in different atmospheres will result in variable discharge capacities. In addition, after 179 cycles, the remaining storage capacities in the S1, S2, S3, and S4 models are 72, 60, 74, and 66 mAh/g, respectively. TNA compounds annealed under oxygen atmosphere showed a higher capacity compared to the argon atmosphere, which can be due to lower compression and higher disorder in the annealed samples under oxygen atmosphere compared to that of argon. The produced anode performances were investigated in different C rates, including 0.1C, 0.2C, 0.5C, 1C, 2C, and 4C (Table 2). Based on Figure 5, the performance of annealed anodes in terms of cyclability and capacity retention is better in the oxygen atmosphere than the annealed anodes under argon.

Table 2. Electrochemical performance of the produced electrodes.

Sample No.	Cycle No.	No. of Cycles per Each C Rate						Capacity (mAh/g)					
		0.1C	0.2C	0.5C	1C	2C	4C	0.1C	0.2C	0.5C	1C	2C	4C
S1	179	4	8	23	48	48	48	231	192	157	124	97	72
S2	179	4	8	23	48	48	48	264	154	104	83	70	60
S3	179	4	8	23	48	48	48	255	193	142	105	86	74
S4	179	4	8	23	48	48	48	199	141	103	86	76	66

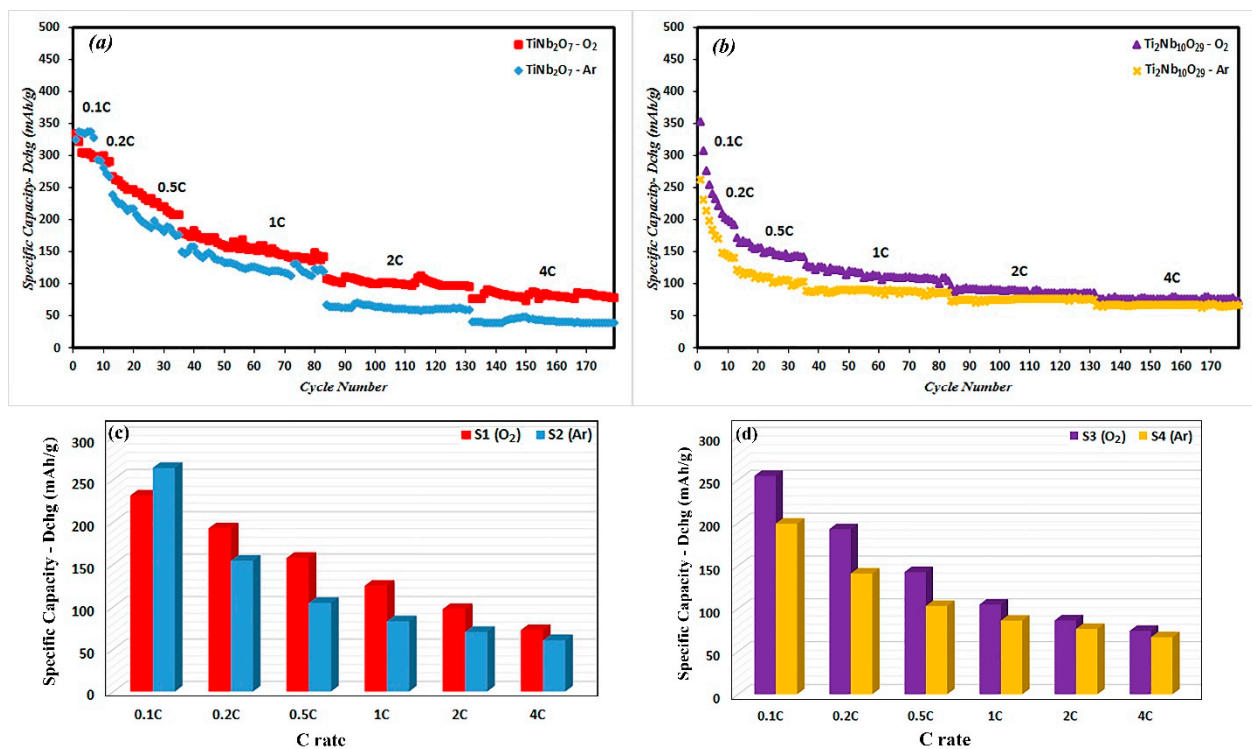


Figure 5. Cycling performance of the Electrodes synthesized in different atmospheres at various charge/discharge rates as indicated (a) TiNb₂O₇, (b) Ti₂Nb₁₀O₂₉, (c,d) bar charts for comparing the discharge capacities at different C rates.

3.2. Electrochemical Properties

The electrochemical impedance (EIS) test is performed when the cell is completely discharged. Figure 6 exhibits the Nyquist diagrams of the annealed samples of TiNb₂O₇ and Ti₂Nb₁₀O₂₉ in two different atmospheres of oxygen and argon (the corresponding curve is placed in the figure for performing the fitting process of the lab data for the EIS test). An intercept is observed at high frequencies, followed by a semicircle in the medium frequency region and a straight line at a low frequency. Ohmic resistors (R_e) include electrolyte and electrode resistors seen as the intercept impedance in the Z' axis. The charging transfer resistors (R_{ct}), available between the anodic material and electrolyte, are in conformity with the diameter of the semicircle on the Z' axis. The tailbone or the straight line is connected with the emission of lithium ions in the electrode bulk [37–44], known as the Warburg diffusion (Z_w). Double layer strength and capacitive surface film are shown as the fixed phase element (CPE) [31].

Table 3 shows the fitting results of the impedance test of the synthesized samples. In this table, the R_{ct} values of the annealed samples in the oxygen atmosphere and the annealed samples in the argon atmosphere are presented for two compounds, TiNb₂O₇ and Ti₂Nb₁₀O₂₉, which in TiNb₂O₇ are equal to 29 and 41 Ω cm² and in Ti₂Nb₁₀O₂₉ are equal to 54 and 979 Ω cm², respectively. There is a significant reduction in the annealed sample under an oxygen atmosphere compared with the annealed sample in the argon atmosphere. Therefore, by calculating the diffusion coefficient of lithium-ion using Equation (3), it was determined that the emission of lithium-ion in the annealed sample under an oxygen atmosphere is faster, so that the diffusion coefficients of the S1 and S2 samples are 1.24×10^{-11} cm²/s and 1.13×10^{-11} cm²/s, respectively. Additionally, this coefficient in samples S3 and S4 is equal to 6.22×10^{-12} cm²/s and 1.49×10^{-14} cm²/s, respectively.

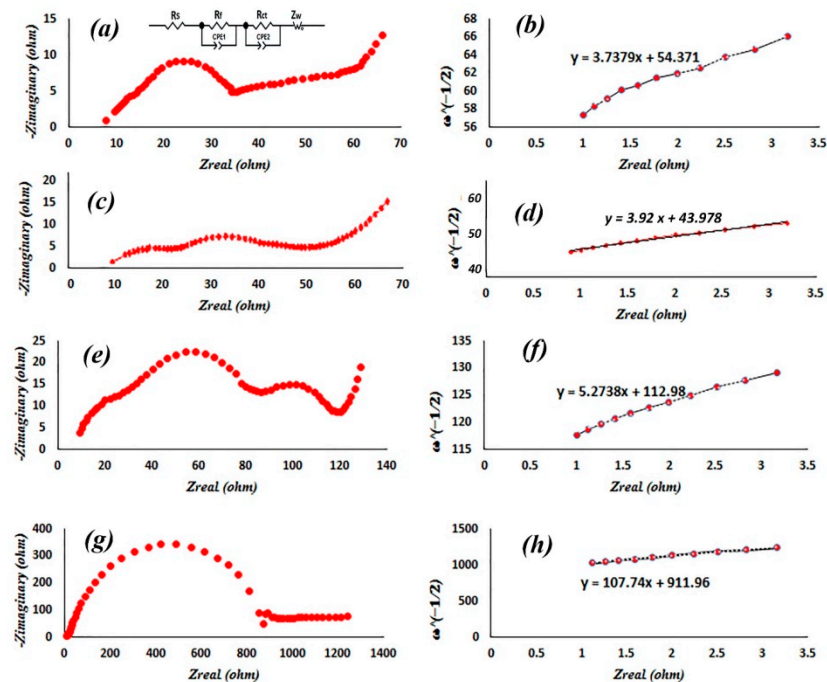


Figure 6. EIS spectra of TiNb_2O_7 and $\text{Ti}_2\text{Nb}_{10}\text{O}_{29}$ annealed under different atmospheres (a,e) oxygen atmosphere, (c,g) argon atmosphere, and equivalent circuit for fitting experimental data, (b,d,f,h) the relationship between Z' and the square root of frequency ($\omega^{-1/2}$) in the low-frequency region for TiNb_2O_7 and $\text{Ti}_2\text{Nb}_{10}\text{O}_{29}$.

The Li-ions diffusion coefficients (D_c) of TiNb_2O_7 composites are extensively investigated in various studies [45–47]. For example, Lin et al. [45] exhibited that the Li-ions D_c of nano- TiNb_2O_7 /carbon tubes composite anode is the order of 10^{-11} cm^2/s . According to Babu et al. [46], the chemical diffusion coefficient of Li-ions in TiNb_2O_7 fluctuates between 10^{-15} and 10^{-16} cm^2/s . The D_c of Li-ions in extremely crystalline TiNb_2O_7 nanoparticles exhibited significant fluctuation between 10^{-12} and 10^{-16} cm^2/s , according to Ise et al. [47]. The D_c of the specimens presented in Table 3 is consistent with other studies findings. The detected disparity in Li-ions diffusion coefficients is attributable to the diverse electrode preparation approaches, the porosity characteristics of the material, and the varied probing approaches utilized. Hence, the quantitative assessment of Li-ions diffusion coefficients via various groups is virtually unfeasible.

Table 3. EIS parameters of the produced electrodes.

Sample	R_e ($\Omega \text{ cm}^2$)	R_{ct} ($\Omega \text{ cm}^2$)	i_0 (mA cm^2)	σ_w ($\Omega \text{ cm}^2 \text{ s}^{1/2}$)	D_c (cm^2/s)
TiNb_2O_7 (O_2)	16.19	29	8.85×10^{-4}	3.74	1.24×10^{-11}
TiNb_2O_7 (Ar)	9.76	41	6.26×10^{-4}	3.92	1.13×10^{-11}
$\text{Ti}_2\text{Nb}_{10}\text{O}_{29}$ (O_2)	20.81	54	4.76×10^{-4}	5.27	6.22×10^{-12}
$\text{Ti}_2\text{Nb}_{10}\text{O}_{29}$ (Ar)	-	-	-	107.74	1.49×10^{-14}

4. Conclusions

In this study, two ceramic compounds, i.e., TiNb_2O_7 and $\text{Ti}_2\text{Nb}_{10}\text{O}_{29}$, were successfully synthesized by mechanical milling method coupled with annealing treatment under different atmospheres, and their electrodes had a significant capacity and cyclability. Performing the annealing treatment in different atmospheres had no influence on the morphology of the synthesized powders. Electrochemical analyses indicated that the annealed samples in an oxygen atmosphere have a higher capacity than their counterparts under argon atmosphere, which can be attributed to less compression and more irregularity in the annealed

samples under an oxygen atmosphere. In addition, the diffusion rate of lithium-ion in the annealed samples under oxygen atmosphere ($1.24 \times 10^{-11} \text{ cm}^2/\text{s}$ in TiNb_2O_7 and $6.22 \times 10^{-12} \text{ cm}^2/\text{s}$ in $\text{Ti}_2\text{Nb}_{10}\text{O}_{29}$) is higher in comparison with the annealed sample in argon atmosphere ($1.13 \times 10^{-11} \text{ cm}^2/\text{s}$ in TiNb_2O_7 and $1.49 \times 10^{-14} \text{ cm}^2/\text{s}$ in $\text{Ti}_2\text{Nb}_{10}\text{O}_{29}$). The result also exhibited that two stoichiometric compositions presented an excellent storage capacity of 72 and 74 mAh/g, respectively, in the oxygen atmosphere after 179 cycles with different C rates.

Supplementary Materials: The following are available online at <https://www.mdpi.com/article/10.3390/met11060983/s1>, Figure S1. EDS analysis of the TiNb_2O_7 and $\text{Ti}_2\text{Nb}_{10}\text{O}_{29}$ compounds, annealed under different atmospheres. Figure S2. FTIR absorption spectra of the TiNb_2O_7 compounds, annealed under different atmospheres.

Author Contributions: Conceptualization, supervision, formal analysis, writing—review and editing, R.E.-K. and H.R.B.-R.; writing—original draft preparation, methodology, formal analysis, T.A.; conceptualization, writing—review and editing, S.M. and M.G.; conceptualization, writing—review and editing, funding acquisition, F.B. All authors have read and agreed to the published version of the manuscript.

Funding: This research received no external funding.

Data Availability Statement: All data provided in the present manuscript are available to whom it may concern.

Conflicts of Interest: The authors declare that they have no competing/financial conflict of interests.

References

1. Larcher, D.; Tarascon, J.-M. Towards greener and more sustainable batteries for electrical energy storage. *Nat. Chem.* **2015**, *7*, 19–29. [[CrossRef](#)]
2. Sun, R.; Liu, G.; Cao, S.; Dong, B.; Liu, X.; Hu, M.; Liu, M.; Duan, X. High rate capability performance of ordered mesoporous $\text{TiNb}_6\text{O}_{17}$ microsphere anodes for lithium ion batteries. *Dalton Trans.* **2017**, *46*, 17061–17066. [[CrossRef](#)] [[PubMed](#)]
3. Lin, C.; Deng, S.; Kautz, D.J.; Xu, Z.; Liu, T.; Li, J.; Wang, N.; Lin, F. Intercalating $\text{Ti}_2\text{Nb}_{14}\text{O}_{39}$ Anode Materials for Fast-Charging, High-Capacity and Safe Lithium-Ion Batteries. *Small* **2017**, *13*, 1702903. [[CrossRef](#)]
4. Yao, F.; Pham, D.; Lee, Y. Carbon-based materials for lithium-ion batteries, electrochemical capacitors, and their hybrid devices. *ChemSusChem* **2015**, *8*, 2284–2311. [[CrossRef](#)] [[PubMed](#)]
5. Liu, Y.; Yang, Y. Recent progress of TiO_2 -based anodes for Li ion batteries. *J. Nanomater.* **2016**, 1–15. [[CrossRef](#)]
6. Croy, J.R.; Balasubramanian, M.; Gallagher, K.G.; Burrell, A.K. Review of the US Department of Energy's "deep dive" effort to understand voltage fade in Li- and Mn-rich cathodes. *Acc. Chem. Res.* **2015**, *48*, 2813–2821. [[CrossRef](#)]
7. Nitta, N.; Wu, F.; Lee, J.T.; Yushin, G. Li-ion battery materials: Present and future. *Mater. Today* **2015**, *18*, 252–264. [[CrossRef](#)]
8. Li, H.; Shen, L.; Pang, G.; Fang, S.; Luo, H.; Yang, K.; Zhang, X. TiNb_2O_7 nanoparticles assembled into hierarchical microspheres as high-rate capability and longcycle-life anode materials for lithium ion batteries. *Nanoscale* **2014**, *7*, 619–624. [[CrossRef](#)] [[PubMed](#)]
9. Catti, M.; Pinus, I.; Knight, K. Lithium insertion properties of $\text{Li}_x\text{TiNb}_2\text{O}_7$ investigated by neutron diffraction and first-principles modelling. *J. Solid State Chem.* **2015**, *229*, 19–25. [[CrossRef](#)]
10. Park, H.; Wu, H.B.; Song, T.; Lou, X.W.; Paik, U. Porosity controlled TiNb_2O_7 microspheres with partial nitridation as a practical negative electrode for high-power lithium-ion batteries. *Adv. Energy Mater.* **2015**, *5*, 1401945. [[CrossRef](#)]
11. Lou, S.; Cheng, X.; Zhao, Y.; Lushington, A.; Gao, J.; Li, Q.; Zuo, P.; Wang, B.; Gao, Y.; Ma, Y.; et al. Superior performance of ordered macroporous TiNb_2O_7 anodes for lithium ion batteries: Understanding from the structural and pseudocapacitive insights on achieving high rate capability. *Nano Energy* **2017**, *34*, 15–25. [[CrossRef](#)]
12. Wang, G.; Wen, Z.; Du, L.; Yang, Y.; Li, S.; Sun, J.; Ji, S. Hierarchical Ti-Nb oxide microspheres with synergic multiphase structure as ultra-long-life anode materials for lithium-ion batteries. *J. Power Sour.* **2017**, *367*, 106–115. [[CrossRef](#)]
13. Zhu, G.; Wang, Y.; Xia, Y. Ti-based compounds as anode materials for Li-ion batteries. *Energy Environ. Sci.* **2012**, *5*, 6652–6667. [[CrossRef](#)]
14. Balasingam, S.K.; Kundu, M.; Balakrishnan, B.; Kim, H.; Sevansson, A.M.; Jayasayee, K. Hematite microdisks as an alternative anode material for lithium-ion batteries. *Mater. Lett.* **2019**, *247*, 163–166. [[CrossRef](#)]
15. Li, S.; Cao, X.; Schmidt, C.N.; Xu, Q.; Uchaker, E.; Pei, Y.; Cao, G. TiNb_2O_7 /graphene composites as high-rate anode materials for lithium/sodium ion batteries. *J. Mater. Chem. A* **2016**, *4*, 4242–4251. [[CrossRef](#)]
16. Xia, X.; Deng, S.; Feng, S.; Wu, J.; Tu, J. Hierarchical porous $\text{Ti}_2\text{Nb}_{10}\text{O}_{29}$ Nanospheres as superior anode materials for lithiumion storage. *J. Mater. Chem. A* **2017**, *5*, 21134–21139. [[CrossRef](#)]
17. Tang, K.; Mu, X.; Aken, P.A.; Yu, Y.; Maier, J. Nano-Pearl-String TiNb_2O_7 as Anodes for Rechargeable Lithium Batteries. *Adv. Energy Mater.* **2012**, *3*, 49–53. [[CrossRef](#)]

18. Jo, C.; Kim, Y.; Hwang, J.; Shim, J.; Chun, J.; Lee, J. Block copolymer directed ordered mesostructured TiNb_2O_7 multimetallic oxide constructed of nanocrystals as high power Li-ion battery anodes. *Chem. Mater.* **2014**, *26*, 3508–3514. [[CrossRef](#)]
19. Lin, C.; Wang, G.; Lin, S.; Li, J.; Lu, L. $\text{TiNb}_6\text{O}_{17}$: A new electrode material for lithium-ion batteries. *Communication* **2015**, *51*, 8970–8973. [[CrossRef](#)]
20. Perfler, L.; Kahlenberg, V.; Wikete, C.; Schmidmair, D.; Tribus, M.; Kaindl, R. Nanoindentation, High-temperature behavior, and crystallographic/spectroscopic characterization of the high-refractive-index materials TiTa_2O_7 and TiNb_2O_7 . *Inorg. Chem.* **2015**, *54*, 6836–6848. [[CrossRef](#)]
21. Pham-Cong, D.; Kim, J.; Tran, V.T.; Kim, S.J.; Jeong, S.; Choi, J.; Cho, C. Electrochemical behavior of interconnected $\text{Ti}_2\text{Nb}_{10}\text{O}_{29}$ nanoparticles for high-power Li-ion battery anodes. *Electrochim. Acta* **2017**, *236*, 451–459. [[CrossRef](#)]
22. Wang, G.; Wang, H.; Ling, Y.; Tang, Y.; Yang, X.; Fitzmorris, R.C.; Wang, C.; Zhang, J.Z.; Li, Y. Hydrogen-treated TiO_2 nanowire arrays for photoelectrochemical water splitting. *Nano Lett.* **2011**, *11*, 3026–3033. [[CrossRef](#)]
23. Hu, S.; Li, F.; Fan, Z. Preparation of dihydroxy naphthalene/ TiO_2 complex via surface modification and their photocatalytic H_2 production performances under visible light. *Bull. Korean Chem. Soc.* **2013**, *34*, 2056–2062. [[CrossRef](#)]
24. Hansen, P.L.; Wagner, J.B.; Helveg, S.; Rostrup-Nielsen, J.R.; Clausen, B.S.; Topsøe, H. Atom-resolved imaging of dynamic shape changes in supported copper nanocrystals. *Science* **2002**, *295*, 2053–2055. [[CrossRef](#)]
25. Lin, J.; Lin, Y.; Liu, P.; Mezziani, M.J.; Allard, L.F.; Sun, Y.P. Hot-fluid annealing for crystalline titanium dioxide nanoparticles in stable suspension. *J. Am. Chem. Soc.* **2002**, *38*, 11514–11518. [[CrossRef](#)]
26. Rai, A.K.; Anh, L.T.; Gim, J.; Mathew, V.; Kang, J.; Paul, B.J.; Song, J.; Kim, J. Simple synthesis and particle size effects of TiO_2 nanoparticle anodes for rechargeable lithium ion batteries. *Electrochim. Acta* **2013**, *90*, 112–118. [[CrossRef](#)]
27. Liu, N.; Schneider, C.; Freitag, D.; Hartmann, M.; Venkatesan, U.; Müller, J.; Spiecker, E.; Schmuki, P. Black TiO_2 nanotubes: Cocatalyst-free open-circuit hydrogen generation. *Nano Lett.* **2014**, *14*, 3309–3313. [[CrossRef](#)] [[PubMed](#)]
28. Liu, D.; Xiao, P.; Zhang, Y.; Garcia, B.B.; Zhang, Q.; Guo, Q.; Champion, R.; Cao, G. TiO_2 nanotube arrays annealed in N_2 for efficient lithium-ion intercalation. *J. Phys. Chem. C* **2008**, *112*, 11175–11180. [[CrossRef](#)]
29. Liu, D.; Zhang, Y.; Xiao, P.; García, B.B.; Zhang, Q.; Zhou, X.; Jeong, Y.-H.; Cao, G. TiO_2 nanotube arrays annealed in CO exhibiting high performance for lithium-ion intercalation. *Electrochim. Acta* **2009**, *54*, 6816–6820. [[CrossRef](#)]
30. Willison, G.K.; Hall, W.H. X-ray Line Broadening from Filled Aluminum and Wolfram. *Acta Metall.* **1953**, *1*, 122–131.
31. Madram, A.R.; Daneshtalab, R.; Sovizi, M.R. Effect of Na^+ and K^+ co-doping on the structure and electrochemical behaviors of LiFePO_4/C cathode material for lithium-ion batteries. *R. Soc. Chem.* **2016**, *6*, 101477–101484. [[CrossRef](#)]
32. Jiang, W.T.; Peacor, D.R.; Rkaip, A.; Toth, M.; Kim, J.W. TEM and XRD Determination of Crystallite Size and Lattice Strain as a Function of Illite Crystallinity in Pelitic Rocks. *J. Metamorph. Geol.* **2004**, *15*, 267–281. [[CrossRef](#)]
33. Reddy, M.; Pralong, V.; Varadaraju, U.V.; Raveau, B. Crystallite Size Constraints on Lithium Insertion into Brookite TiO_2 . *Electrochem. Solid State Lett.* **2008**, *11*, A132–A134. [[CrossRef](#)]
34. Liu, Y.; Liu, D.; Zhang, Q.; Cao, G. Engineering nanostructured electrodes away from equilibrium for lithium-ion batteries. *J. Mater. Chem.* **2011**, *21*, 9969–9983. [[CrossRef](#)]
35. Liu, D.; Liu, Y.; Garcia, B.B.; Zhang, Q.; Pan, A.; Jeong, Y.-H.; Cao, G. V_2O_5 xerogel electrodes with much enhanced lithium-ion intercalation properties with N_2 annealing. *J. Mater. Chem.* **2009**, *19*, 8789–8795. [[CrossRef](#)]
36. Griffith, K.J.; Seymour, I.D.; Hope, M.A.; Butala, M.M.; Lamontagne, L.K.; Preefer, M.B.; Koçer, C.P.; Henkelman, G.; Morris, A.J.; Cliffe, M.J.; et al. Ionic and Electronic Conduction in TiNb_2O_7 . *J. Am. Chem. Soc.* **2019**, *141*, 16706–16725. [[CrossRef](#)] [[PubMed](#)]
37. Gerold, E.; Luidold, S.; Antrekowitsch, H. Selective Precipitation of Metal Oxalates from Lithium Ion Battery Leach Solutions. *Metals* **2020**, *10*, 1435. [[CrossRef](#)]
38. Jenei, P.; Kádár, C.; Han, G.; Hung, P.T.; Choe, H.; Gubicza, J. Annealing-Induced Changes in the Microstructure and Mechanical Response of a Cu Nanofoam Processed by Dealloying. *Metals* **2020**, *10*, 1128. [[CrossRef](#)]
39. Brückner, L.; Frank, J.; Elwert, T. Industrial Recycling of Lithium-Ion Batteries—A Critical Review of Metallurgical Process Routes. *Metals* **2020**, *10*, 1107. [[CrossRef](#)]
40. Cho, Y.; Kim, K.; Ahn, J.; Lee, J. Application of Multistage Concentration (MSC) Electrodialysis to Concentrate Lithium from Lithium-Containing Waste Solution. *Metals* **2020**, *10*, 851. [[CrossRef](#)]
41. Klimko, J.; Oráč, D.; Miškuřová, A.; Vonderstein, C.; Dertmann, C.; Sommerfeld, M.; Friedrich, B.; Havlík, T. A Combined Pyro- and Hydrometallurgical Approach to Recycle Pyrolyzed Lithium-Ion Battery Black Mass Part 2: Lithium Recovery from Li Enriched Slag—Thermodynamic Study, Kinetic Study, and Dry Digestion. *Metals* **2020**, *10*, 1558. [[CrossRef](#)]
42. Schwich, L.; Küpers, M.; Finsterbusch, M.; Schreiber, A.; Fattakhova-Rohlfing, D.; Guillon, O.; Friedrich, B. Recycling Strategies for Ceramic All-Solid-State Batteries—Part I: Study on Possible Treatments in Contrast to Li-Ion Battery Recycling. *Metals* **2020**, *10*, 1523. [[CrossRef](#)]
43. Schwich, L.; Sabarny, P.; Friedrich, B. Recycling Potential of Lithium–Sulfur Batteries—A First Concept Using Thermal and Hydrometallurgical Methods. *Metals* **2020**, *10*, 1513. [[CrossRef](#)]
44. Sinn, T.; Flegler, A.; Wolf, A.; Stübinger, T.; Witt, W.; Nirschl, H.; Gleiß, M. Investigation of Centrifugal Fractionation with Time-Dependent Process Parameters as a New Approach Contributing to the Direct Recycling of Lithium-Ion Battery Components. *Metals* **2020**, *10*, 1617. [[CrossRef](#)]
45. Lin, C.; Hu, L.; Cheng, C.; Sun, K.; Guo, X.; Shao, Q.; Li, J.; Wang, N.; Guo, Z. Nano- TiNb_2O_7 /carbon nanotubes composite anode for enhanced lithium-ion storage. *Electrochim. Acta* **2018**, *260*, 65–72. [[CrossRef](#)]

-
46. Babu, B.; Shaijumon, M.M. Studies on kinetics and diffusion characteristics of lithium ions in TiNb_2O_7 . *Electrochim. Acta* **2020**, *345*, 136208. [[CrossRef](#)]
 47. Ise, K.; Morimoto, S.; Harada, Y.; Takami, N. Large lithium storage in highly crystalline TiNb_2O_7 nanoparticles synthesized by a hydrothermal method as anodes for lithium-ion batteries. *Solid State Ion.* **2018**, *320*, 7–15. [[CrossRef](#)]